

# A Database of Underwater Radiated Noise from Small Vessels in the Coastal Area

---

**Shipton, Mark; Obradović, Juraj; Ferreira, Fausto; Mišković, Nikola; Bulat, Tomislav; Cukrov, Neven; Diamant, Roe**

*Source / Izvornik:* **submitted to Scientific Data, 2024**

**Journal article, Submitted version**

**Rad u časopisu, Rukopis poslan na recenzijski postupak (preprint)**

*Permanent link / Trajna poveznica:* <https://um.nsk.hr/um:nbn:hr:168:030404>

*Rights / Prava:* [In copyright](#)/[Zaštićeno autorskim pravom](#).

*Download date / Datum preuzimanja:* **2024-12-27**



*Repository / Repozitorij:*

[FER Repository - University of Zagreb Faculty of Electrical Engineering and Computing repository](#)



# A Database of Underwater Radiated Noise from Small Vessels in the Coastal Area

Mark Shipton<sup>1,+</sup>, Juraj Obradović<sup>2,+</sup>, Fausto Ferreira<sup>2</sup>, Nikola Mišković<sup>2</sup>, Tomislav Bulat<sup>3</sup>, Neven Cukrov<sup>3</sup>, and Roe Diamant<sup>1,2,\*</sup>

<sup>1</sup>University of Haifa, Department of Marine Technology, Haifa, 3498838, Israel

<sup>2</sup>University of Zagreb, Faculty of Electrical Engineering and Computing, Zagreb, Unska 3, Croatia

<sup>3</sup>Division for marine and environmental research, Ruder Bošković Institute, Zagreb, 10000, Croatia

<sup>+</sup>equal contribution

<sup>\*</sup>Corresponding author: Roe Diamant, roee.d@univ.haifa.ac.il

## ABSTRACT

The current procedures for measuring underwater radiated noise (URN) are designed for cooperating vessels in controlled areas. As such, not a lot of data is available for the URN of unidentified vessels of opportunity (VOO), especially for small vessels that do not carry an automatic identification systems (AIS). To this end, we assembled a database of 1148 VOO's URN from acoustic and visual recordings of ferries, fishing boats, yachts, and small speed boats made within Šibenik canal, Croatia. The database comprises source pressure levels at the closest point of approach, picture and video of the vessel, and the vessel's speed, size, and type. A shared webpage allows filtering and comparing vessel types and characteristics. To the best of our knowledge, this is one of the largest databases of vessel URN in general and the most extensive database for small coastal vessels. In this paper, we share the structure of our database, the analysis methodology. We conclude that the URN of small vessels is significant and comparable to large vessels.

## Background & Summary

Underwater radiated noise (URN) from shipping activity has been identified as a significant component of ocean ambient noise<sup>1-3</sup>, with recent studies indicating that URN doubles in intensity every decade. The effects of URN on various components of the marine ecosystem, from mussels to marine mammals, have been extensively studied across disciplines<sup>4</sup>. Several reports (e.g.,<sup>5,6</sup>) suggest that blunt tissue trauma comparable to blast injuries and behavioral changes reflected in social stability and foraging ability have the potential to affect aquatic animals residing in close proximity to a vessel emitting high sound intensities from its propellers or onboard engines. Research has shown that URN from vessel activity leads to a myriad of adverse effects on fish, crustaceans, and especially on cetaceans<sup>4,7-10</sup>. In particular, the responses of a given aquatic animal to anthropogenic noise can be divided into five main categories<sup>11</sup>: (I) audibility; (II) behavioral responses reflected in changes in the intensity, frequency and intervals of the animal's vocalizations as well as stress behavior; (III) masking of sounds required for communication, localization and foraging; (IV) physiological auditory threshold shifts due to inner ear hair cell fatigue; and (V) physical damage (injury) to the auditory system. In addition, there are direct risks associated with physical disturbance, as in the cases where sea turtles<sup>12</sup> and large baleen whales<sup>13</sup> colliding with vessels, partly because the low-frequency sounds from ships interfere with their navigation. Because of these effects, URNs generated by ships are considered a source of pollution and should be monitored regularly by measuring ship noise.

Shipping URN includes high-power impulsive transient waves generated during ignition<sup>14</sup>, narrow-band noises generated from thrusters, engines as well pumps and generators<sup>15</sup>, and cavitation noises. The latter is caused by the fast enough turn of the propeller to allow low-pressure areas of the propeller to drop below the vapor pressure and the seawater to *boil* at ambient temperature. When the bubbles reach ambient pressure behind the propeller, they implode, yielding broadband stationary noise. The results are: (1) low-frequency noise (around 50 Hz, distributed over a huge area, which impacts the communication of large marine mammals like baleen whales and dolphins); (2) noise from 4-stroke engines (around 200-800 Hz, independent of speed, medium distribution, which likely impacts toothed whales); and (3) high-frequency noise with higher harmonics due to the Lloyd's mirror effect<sup>16</sup> (1 kHz-10 kHz, speed-dependent, which can bear a significant amount of acoustic energy, and likely effects small mammals and fish).

Standards have been established to limit the transmitted acoustic power per exposure time<sup>17</sup>, and regulatory organizations such as the European Union, the Convention on the Conservation of Migratory Species (CMS), and the Convention on Biological Diversity (CBD), have adopted resolutions aimed at reducing underwater noise from ships and other man-made noise sources. There have even been recent efforts by the shipping industry to reduce URN by creating specialized notations for ships that

40 meet certain noise criteria<sup>18</sup>. Although there are standards for quantifying the URN of vessels<sup>19</sup>, these require the cooperation  
41 of the ship: sailing on a fixed route and at nominal speed. The measurement is carried out at deep sea and under low-noise  
42 conditions. These conditions do not apply to the URN measurement of a vessel of opportunity (VOO). Specifically, vessels that  
43 are not obliged or avoid carrying an automatic identification system (AIS). As a result, the magnitude of noise from such vessels  
44 remains under-explored, and a quantitative study examining the extent of shipping URN has yet to be thoroughly conducted.  
45 The main barrier to such studies is the establishment of a proper approach to match the size and type of a vessel to its URN.

46 In this paper, we have addressed the challenge of quantifying the URN of VOO by integrating acoustic measurements with  
47 video footage processed using machine learning to estimate the vessel's type, speed, and size. This negated the need to detect  
48 the vessel's URN in the acoustic data, and the closest point of access (CPA) could be readily analyzed by time synchronization  
49 of the optical and acoustic data. The results of our work is an openly shared dictionary for URN of VOO. The data was collected  
50 at the entrance to St. Anthony's Channel near Šibenik, Croatia. Through this channel, a daily traffic of hundreds of vessels  
51 exists. Most of these vessels do not carry an AIS but are easy to observe visually as they enter or exit the channel. In total, 1148  
52 vessels were assessed over a period of 23 days. Our data comprises pictures and videos of the vessels, the spectrum of their  
53 URN at the CPA, and meta-data in the form of the vessel's type, size, height, and speed. In the following, we outline our data  
54 collection method, the details of the database and its front-end tool that allows comparison of shipping URN.

### 55 **Current Approaches in Shipping Noise Measurement**

56 The literature regarding URN measurement focuses on assessing the noise levels and spectral characteristics of various vessel  
57 types under different operating conditions (e.g., speed, cargo load, draft, length, and machinery load). There are currently two  
58 main approaches for assessing URN from vessels; the first is a "full-control" approach where specific vessels are chartered to  
59 conduct measurements under specified operating conditions<sup>20-22</sup>. This approach requires near full control over the measurement  
60 and operating conditions (e.g., speed of the vessel, CPA range), thereby enabling highly accurate measurements as well  
61 as the ability to conduct repetitive measurements of the same vessel under different operating conditions. However, the  
62 cost-effectiveness of this approach also implies that usually, only a small number of vessels is assessed. The second and more  
63 prominent approach is the "opportunistic" or *in situ* approach, where sensors and data collecting units are placed near main  
64 waterways, and measurements of VOOs are acquired as they transit the area<sup>23-25</sup>. While the *in situ* approach lacks the ability to  
65 control the measurement or operating conditions, it does enable the collection of a larger sample number over longer periods of  
66 time.

67 The most common methodology utilized in both the full-control and the *in situ* approaches is cross-referencing acoustic  
68 data collected by hydrophones with vessel data. In this aspect, the introduction of the Automatic Identification System (AIS)  
69 in the early 2000s has created an accessible and convenient venue for collecting vessel data. The bulk of current research  
70 frameworks have primarily depended on AIS for retrieving vessel data<sup>23,26-28</sup>. While the widespread use of AIS creates more  
71 opportunities for full-control and opportunistic URN assessments, it is also important to point out its inherent limitations - as  
72 noted in the SOLAS regulation V/19.2<sup>29</sup>, AIS transponders are a legal requirement only for large commercial vessels, e.g.,  
73 cargo vessels, tankers, passenger ships. This implies that smaller commercial and recreational vessels that are abundant in  
74 coastal areas are mostly absent from the current research agenda. The importance of this absence is further emphasized by  
75 two aspects. Firstly, the numerical comparison between the number of large commercial vessels and the number of small  
76 recreational vessels - the world's total fleet of large commercial vessels is comprised of nearly 109,000 ships<sup>30</sup>, while there are  
77 nearly 12 million recreational vessels in the US alone<sup>31</sup>. Secondly, the scarce research that has addressed URN from small  
78 recreational vessels suggests that under certain conditions, URN from such vessels may be as high or even exceed those of  
79 large commercial vessels<sup>26,32,33</sup>. Accordingly, it would seem imperative that a novel approach for assessing URN from smaller  
80 vessels is required to fill this gap.

81 The main challenge for conducting wide-scale assessments of small vessels not equipped with AIS is the retrieval of vessel  
82 data in order to collect information on the vessel's type, speed, size, and CPA range. This is available through sensors such as  
83 radar and HD cameras. Cope et al.<sup>32</sup>, for example, utilized a multi-sensor system (Marine Monitor - M2) comprised of AIS,  
84 Radar, and an HD camera for assessing URN levels of vessels. While this approach enables retrieving essential vessel data such  
85 as vessel speed, course, and CPA range, other important parameters, such as vessel size, cannot be accurately assessed. To  
86 account for the need to collect acoustic data as well as detailed vessel information accurately, we propose a novel approach  
87 based on the integration of acoustic and optical sensors.

### 88 **Current Approaches in Vessel Detection from Optical Cameras**

89 The methods for detecting ships using cameras are designed to cope with motion and observation noise. The vessel detection  
90 approach in<sup>34</sup> performs background subtraction to detect primary motion in the scene while avoiding interference from wave  
91 motion using saliency detection. Similarly, in<sup>35</sup>, the authors propose a video-based port surveillance that combines context  
92 and motion detection. The context part of the algorithm involves graph-based segmentation to identify the ship within the  
93 water region, while the motion saliency algorithm utilizes the faster motion of the ship relative to its surroundings. A different

94 approach is proposed in<sup>36</sup>, where eigenvalues of region covariance are computed to distinguish man-made objects from the  
95 natural background. Another type of scene separation using optical flow is proposed in<sup>37</sup> to estimate the moving region in  
96 the image, and a Gabor filter is implemented for extracting texture features indicating where the ships are located. However,  
97 different possible vessel types make it difficult to achieve robust detection and classification.

98 Due to changing visibility conditions and different shapes of vessels, solutions have recently been developed to identify  
99 ships with optical cameras using machine learning methods. These require training with large data sets. For example, the  
100 dataset provided in<sup>38</sup> contains 5,500 ship images of 109 different classes taken in the Porto Cesareo Marine Protected Area.  
101 Results of ship identification using a discriminatively learned CNN are presented. Another dataset is available in<sup>39</sup>, comprising  
102 70,513 vessels, which were recorded in 48,966 images from 10 camera perspectives. As a basis for vessel identification, the  
103 authors propose the Single Shot Detector (SSD) algorithm, which supports significant variations in vessel size and aspect ratios.

104 Current approaches to vessel identification are based on transfer learning from already trained models. In<sup>40</sup>, the YOLOv3-  
105 tiny network is used to recognize vessels and distinguish between six vessel types. For the detection of large vessels, which  
106 are easily disturbed by surrounding buildings, waves and lights on the water surface, the Convolutional Block Attention  
107 Module (CBAM) is used to focus the model on the target vessel. In<sup>41</sup>, the YOLOv5XL model is used to fuse camera data  
108 with AIS information. Through transfer learning, only the last layer was trained with annotated data, which contributes to the  
109 generalization of the model. Another application of the YOLOv5 network is presented in<sup>42</sup> to classify between vessel types.

110 What distinguishes our work from previous work in vessel detection from optical cameras is the use of the YOLOv5  
111 network to detect different types of vessels traveling through narrow canals, and to estimate their size and speed. This system  
112 provides more information about the vessel than a bounding box within the image and can manage multiple vessels within a  
113 single image. This additional information is used to establish a better link between the vessel's URN and its characteristics and  
114 to monitor maritime traffic in narrow areas such as canals, channels, and entrances to marinas with high shipping activity.

## 115 **Methods**

### 116 **Visual Analysis**

117 Using shore-fixed camera, we attempt to estimate the size, type and speed of any VOO passing through the Šibenik channel. To  
118 this end, we develop a machine learning based model for vessel detection, tracking and classification from video footage. The  
119 model provides a bounding box around the vessel. The algorithm then estimates the meter/pixel ratio and determines the size  
120 of the boat in meters from the width of the bounding box. In turn, the tracking procedure follows the bounding box through  
121 consecutive frames to estimate the vessel's velocity.

### 122 ***Vessel Detection and Classification***

123 For detection, we used the YOLOv5-based trained model which is a fast training model. The details of this implementation  
124 are presented in<sup>43</sup> and are given here in brief for completion. The YOLOv5s model is the second smallest of the YOLOv5  
125 family<sup>44</sup>. The model includes a backbone based on Darknet53 with Cross Stage Partial (CSP)<sup>45</sup>, namely 2 BottleNeckCSP  
126 modules and one Spatial Pyramid Pooling (SPP)<sup>46</sup> block (SPPF) with max pooling (kernel pool size = 5) and a neck based on  
127 the Path Aggregation Network (PANet). All convolutional layers used a Sigmoid Linear Unit (SiLU) activation function and  
128 batch normalization except the three layers that form the head of the network (Sigmoid function).

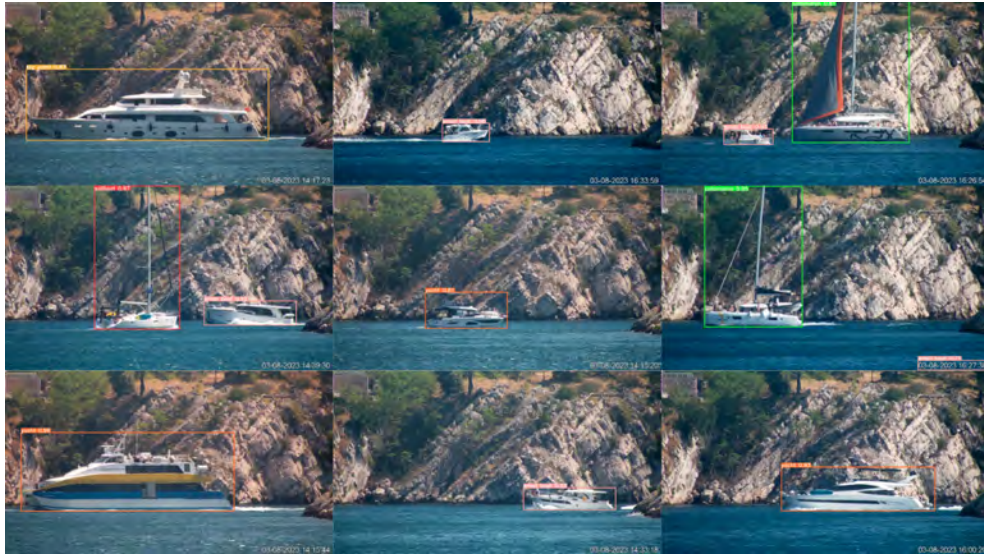
129 The model detects and classifies vessels into 9 classes: sailboat, catamaran, small boat, yacht, big yacht, tour boat, passenger  
130 boat, trawler, medium boat. For vessel detection and classification, the model was trained using 2100 manually labeled images,  
131 observed in 4 different days, and was validated and tested with 100 and 300 images, respectively, captured on days unrelated to  
132 the training dataset. Tuned hyper parameters yielded 100 epochs and a batch size of 8. Challenges occur in edge cases when  
133 a boat exits the frame, causing the bounding box to start shrinking. Avoiding this, we define a region of interest (ROI) that  
134 isolates edge positions.

### 135 ***Vessel Size Estimation***

136 To determine the meter/pixel conversion rates, we used as ground truth 10 vessels from the collected visual data for which the  
137 size is known by factory specifications. This small dataset included speedboats, catamarans and tourist boats for which the size  
138 can be easily found online. For each boat, up to 3 images were identified showing the vessel in the beginning, middle, and end  
139 of the frame. The meter/pixel ratio was calculated for each of the 10 vessels as the relation between real vessel length and  
140 detection bounding box width. A list of all occurrences for the explored 10 vessels is given in Table 1, and examples of the  
141 used frames are given in the Fig. 1.

**Table 1.** Boat Dimensions and Pixel Coefficients

Model	Length [m]	Pixel Width	Average Pix. Width	Coefficient	Err to average
Galeon 640 fly	19.81	0.467, 0.467, 0.47, 0.462	0.466	42.438	0.427
Exess 15	14.63	0.366, 0.355	0.361	40.504	2.361
Lagoon 42	12.8	0.295, 0.301, 0.296	0.298	42.940	-0.0745
Antares 650	6.3	0.145, 0.142, 0.144	0.144	43.667	-0.802
Exess 15	14.63	0.359, 0.360, 0.354	0.358	40.827	2.037
Merry F. 1095	10.5	0.248, 0.242	0.245	42.711	0.153
Mali princ	20	0.659, 0.648	0.653	30.585	12.280
Aloha yacht	32.56	0.736	0.736	44.1803	-1.314
Marex 375	12.05	0.280, 0.275, 0.255	0.270	44.549	-1.683
Greenline 40	12.0	0.280, 0.265	0.272	43.969	-1.104
<b>Average coefficient</b>				42.8655	
<b>Standard deviation</b>				1.3485	

**Figure 1.** Image detections of the boats used for the estimation of meter/pixel coefficient).**142 Velocity estimation**

143 For estimating the vessel's speed, we applied the SORT (Simple Online and Realtime Tracking) approach<sup>47</sup>, which is based on  
 144 Kalman filtering. For vessel dynamics, we consider a constant velocity model. We choose SORT due to its ability to maintain  
 145 track albeit loos of detection for a few frames. This is a typical scenario in our database due to occlusion events where vessels  
 146 cross each other entering or existing the canal. The speed of the vessel is calculated by the distance between the bounding  
 147 boxes at consecutive frames, while accounting for the estimated pixel/meter ratio.

**148 Vessel Noise Estimation****149 Quality Control**

150 Vessel transits were subjected to quality control on three levels: 1) cross-referencing the data with the HD camera, 2) manually  
 151 reviewing acoustic samples by an expert analyst, and 3) monitoring real-time weather information. Samples were discarded  
 152 from the post-analysis under the following criteria.

- 153 1. A vessel transit occurred between recording segments;
- 154 2. Transit occurred in a time frame where wind speed or sea state exceeded ANSI and ISO standards;
- 155 3. If a vessel was employing an active acoustic system (e.g., echo-sounder/Fish-Finder);

- 156 4. If a vessel abruptly changed its course or speed;
- 157 5. If a vessel conducted a north/south transit and did not enter or exit the channel;
- 158 6. If another vessel transited the area within the same time frame;
- 159 7. If a marine fauna noise was detected during the vessels transit.

160 To calculate the vessel's source level, SL, we reverse-propagate the received acoustic signal, accounting for the transmission  
 161 loss, TL, to an idealized monopole @ 1m from the source according to ISO standards<sup>48</sup>, such that

$$162 \quad \text{SL} = \text{SPL} + \text{TL} . \quad (1)$$

162 This requires the calculation of the SPL and the transmission loss as follows.

### 163 **Received Noise Levels**

164 Received noise levels (RL) measurements were conducted for the full spectrum of 0.023–24 kHz. The upper-frequency limit is  
 165 set by the sampling rate, while the lower limit accounts for the cutoff frequency resulting from the water depth according to<sup>49</sup>,

$$166 \quad f_0 = \frac{c}{4D\sqrt{1 - (c/c_b)^2}} , \quad (2)$$

166 where  $c$  is the sound speed in water,  $c_b$  is the sound speed in the seabed, and  $D$  is the water depth.

167 The time window length used for URN evaluation, which is an essential aspect of the measurement, varies across different  
 168 research frameworks. The approach applied in Pine et al.<sup>50</sup> and Zhang et al.<sup>27</sup>, for instance, utilized a constant time window  
 169 length with no dependence on the length, speed, or range of the vessel. Other approaches chose to apply a variable time window  
 170 depending on the vessel's physical characteristics. For example, in Bahtiarian et al.<sup>51</sup> and McKenna et al.<sup>23</sup>, the selected time  
 171 window was dependent on the time it takes for a vessel to travel its length. Unfortunately, neither of these options is suitable for  
 172 our setup. In particular, as the results in Figs. 8, 9 show, our database includes significant variances in vessel transit speeds and  
 173 lengths. Instead, we chose to follow the ISO<sup>48</sup> standard, which sets a variable time window dependent on the aspect of each  
 174 vessel (60–120 deg of the bow aspect). Here, the time window length was calculated based on the vessel's speed, as reported by  
 175 the visual algorithm.

176 To measure the SPL, we applied (3); the variable time window used for the measurement of each vessel transit was processed  
 177 in the frequency domain by a fast-Fourier transform (2048 FFT points, Hanning window with a 50% overlap)<sup>1</sup>.

$$178 \quad \text{SPL} = 20\log_{10} \left( \frac{P_{\text{RMS}}}{P_{\text{ref}}} \right) , \quad (3)$$

178 Where  $P_{\text{ref}} = 1 \mu\text{Pa}$  and  $P_{\text{RMS}}$  is the root mean square of the sound pressure level measured within the variable time window.  
 179 For the measurement of third-octave bands, we applied the same parameters, albeit with a higher frequency resolution (32,768  
 180 FFT points), in order to comply with standard one-third octave bands according to the ANSI Standard S1.11-2014/Part 1<sup>54</sup>.

### 181 **Transmission Loss**

182 The acoustic transmission loss depends on the range of the vessel, geometric spreading characteristics, and the seabed and water  
 183 column properties<sup>55</sup>. Referring to the vessel's range, while the entrance to the inlet is measured at 135.7 m, our observations  
 184 showed that nearly all marine traffic passes through a ~90 m lateral area in the middle of the channel inlet. These observations  
 185 coincide with known hazards to safe navigation and official maritime routes described in maritime charts. Based on this  
 186 information, we calculate the maximum potential CPA range as the slant between the hydrophone and the described lateral  
 187 area (49 m) and the minimum potential CPA range as 29 m (water depth to hydrophone). For the geometric transmission loss  
 188 calculations, we applied the mean CPA range (39 m). This  $\pm 10$  m ambiguity in the vessel's location can be compared with the  
 189 location error of URN databases relying on AIS information, which is known to present a mean discrepancy of up to 97.72 m<sup>56</sup>.

190 In the aspect of absorption losses, applying Ainslie and McColm's<sup>57</sup> equation for absorption in seawater for the mean  
 191 CPA range under different scenarios of temperature and salinity found in the tested area, we reach a maximum loss of roughly  
 192 0.15 dB at the mean CPA range. We, therefore, consider absorption losses as negligible.<sup>2</sup> As the type of sediment in the test

<sup>1</sup>The 2048 FFT resolution was chosen to allow comparability with other research frameworks<sup>52,53</sup>.

<sup>2</sup>Similar conclusions about the negligibly of absorption losses in URN levels of vessels at close ranges have been made in Hermann et al.<sup>58</sup> and McKenna et al.<sup>23</sup>.

193 bed area consists primarily of fine gravel<sup>59</sup>, which possesses a high reflective coefficient<sup>22</sup>, we chose to apply the simplified  
194 equation described by Erbe<sup>60</sup>, which has also been used in similar research frameworks<sup>61</sup>,

$$TL = 20\log_{10}(D) + 10\log_{10}(R/D), \quad (4)$$

195 where  $R$  is the horizontal range between the mean CPA and the receiver and we recall that  $D$  is the water depth.

## 196 Data Records

197 The collected data was arranged in a front-end called "Hear My Ship", that is available in<sup>62</sup>. The web tool allows separation  
198 by vessel's type, speed, length and noise, visualization of the data (both optics and acoustics, data download and comparison  
199 between the URNs of different vessels. In this section we describe the functionality of this front-end.

### 200 Arrangement of Data files

#### 201 Visual Information

202 The optical dataset is organized into 12 folders, each named according to the starting time of the recording in the format  
203 yyyyymmdd\_hhmmss. Each folder contains pairs of 1-hour video files and corresponding .csv files. In total, there are 324 .csv  
204 files. Each .csv file contains detection information with the following columns:

- 205 • `time_of_detection`: The time at which the detection occurred.
- 206 • `boat_class`: The class of the detected boat.
- 207 • `size`: The size of the detected boat.
- 208 • `velocity`: The velocity of the detected boat.

An example for the visual data architecture is shown in Fig. 2.

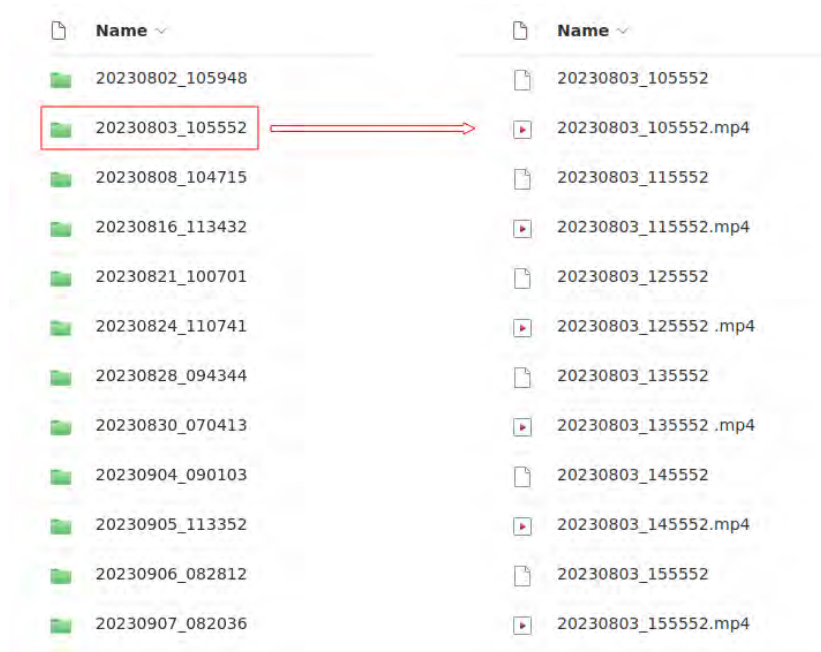


Figure 2. Organisation of the visual data.

209

### 210 Acoustic Information and Online Database

211 The acoustic dataset and processed acoustic information include the time and date of transit, the type of vessel, the sub-type of  
212 the vessel, the length and speed of the vessel (according to the visual algorithm), the calculated SL-SPL, and one-third octave  
213 spectrogram, and, where applicable, the full name and IMO number.

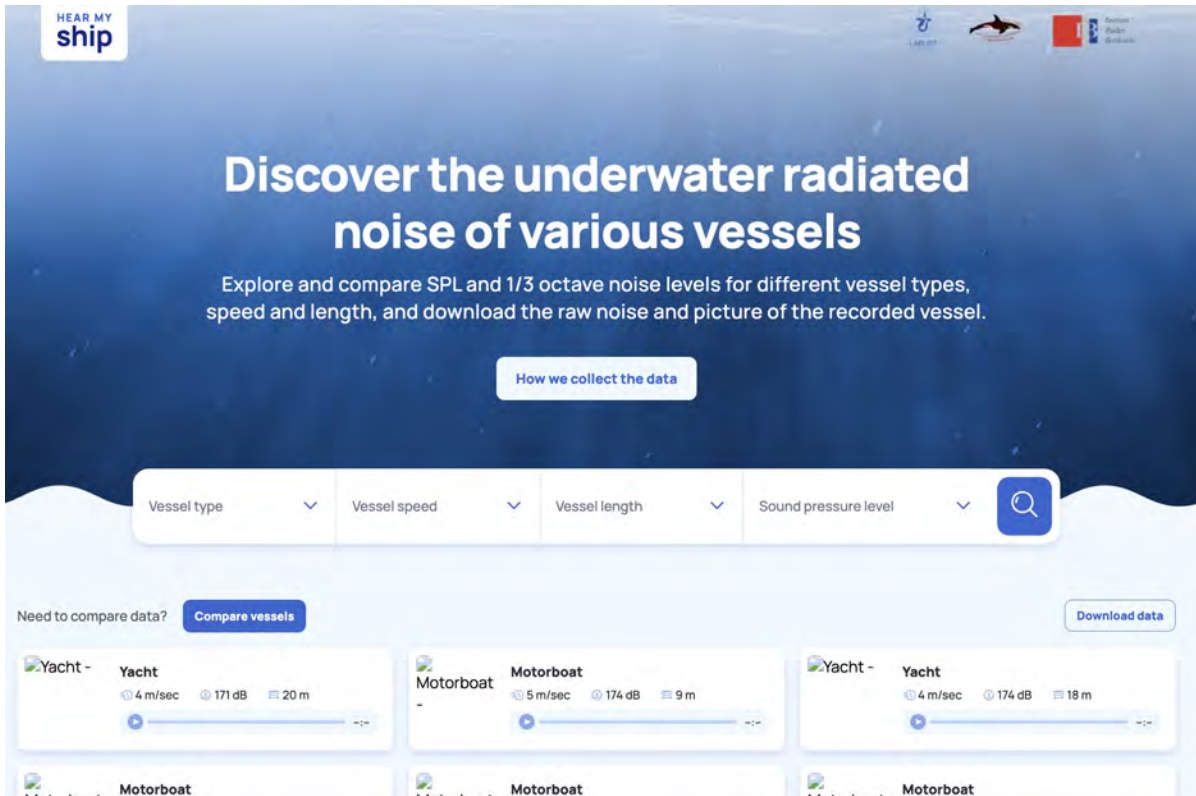
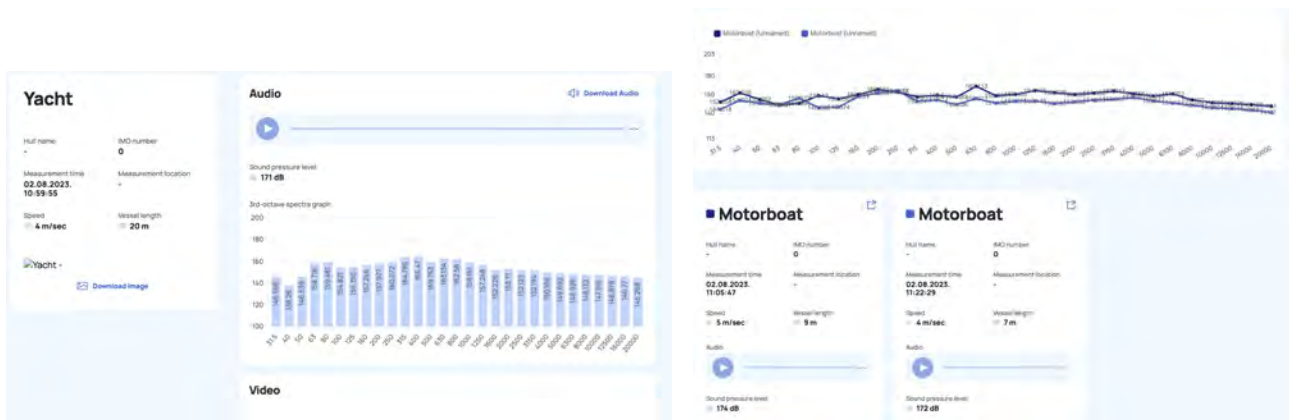


Figure 3. Landing page of the "Hear My Ship" Database Website

215 The landing page of the front end is shown in Fig. 3, and the web page is available in<sup>62</sup>. The link to "How we collect the  
 216 data" refers to this manuscript. Four selection tabs allow the user to filter the data by the desired vessel type (e.g., ferry or  
 217 motorboat), vessel speed (in m/s), vessel length (in m), and SPL (in dB). Several selections are possible in each category. A  
 218 click on the search field on the right displays all vessels that match the search criteria. Clicking on each of these entries will  
 219 open a window similar to Fig. 4a, showing the details of the selected vessel as well as the option to listen to and download the  
 220 recording URN and video. The window also shows the calculated SPL and the 3rd-octave spectrum level.



(a) Example of a vessel entry window.

(b) Example of a vessel comparison page.

Figure 4. Examples from the "Hear My Ship" front-end.

221 Another functionality is the comparison between different vessels with the option "Compare vessels" on the landing page.



222 Clicking this option allows the user to select up to five vessels from the filtered list. After selecting and clicking again on the  
223 "Compare vessels" option, another window is displayed, similar to the example in Fig. 4b. This window shows the details of the  
224 selected vessels and a diagram comparing the spectrum of the vessels' URNs. Finally, clicking the "download data" option  
225 in the landing page, downloads a .json file with all the details of the filtered vessels. For each entry in this file, the user will  
226 receive the details of the vessel, its analyzed SPL and spectrum, a link to download the .wav file with the URN recordings and a  
227 link to download the 10 s video recordings of the vessel.

## 228 Technical Validation

### 229 Description of the Testbed

230 Our testbed resides in the area of St. Anthony's Channel (Sv. Ante in local dialect) Inlet near Šibenik, Croatia. During the  
231 summertime, the area is characterized by high-density shipping, which includes various classes of vessels, ranging from coastal  
232 commercial ferries to smaller recreational vessels, e.g., yachts, motorboats, and sailboats. These conditions make the area  
233 an ideal testbed for analyzing underwater radiated noise from vessels that are not obligated to carry AIS transponders. An  
illustration of the testbed is shown in Fig. 5a.



(a) Illustration of the acoustic-optic testbed for quantifying the URN of VOO by using synchronized optical measurements from a shore-based camera and an acoustic recorder positioned at the seabed.



(b) Picture of the underwater acoustic recorder at the deployment site.

Figure 5. The "Tour boat" category.

234

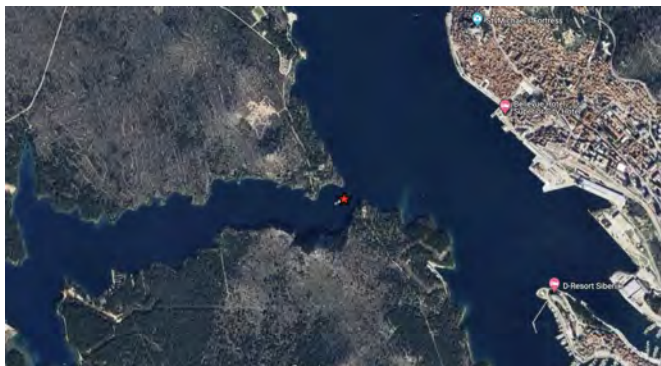


Figure 6. A satellite image of the deployment site. The recorder location is marked in red (right next to the vessel in the image).

235 On August 2023, an AMAR G3 JASCO acoustic recorder with a single M36-V35-900 Geospectrum omnidirectional  
236 hydrophone was placed near the eastern entrance to the Channel Inlet at coordinates  $43.728400^\circ$ ,  $15.879271^\circ$  (see map in  
237 Fig. 6). The hydrophone had a flat with max 0.5 dB ripple response between 0.01-100 kHz and sensitivity of -164.9 dB

238 re:1V/ $\mu$ Pa. At the point of deployment, the channel is 130.3 m wide and most vessels pass in the middle of the channel. The  
 239 recorder was mounted vertically to an anchor one meter above the seabed at a depth of 29 m. The hydrophone's cage was  
 240 covered by a dense yellow net to reduce flow noise and assist in locating the recorder after three months of deployment, as  
 241 shown in Fig. 5b. The recorder was set to record continuously for 12 hours a day between 7:00 to 19:00 (UTC+2) to account  
 242 for daylight hours for the specified region at the time of deployment. The recording was made at a sampling rate of 48 kbps, in  
 243 a resolution of 3 Bytes per sample. In total, 661 GB were recorded over a period of 113 consecutive days.

244 A DAHUA SD-59230U-HNI (30x optical zoom) video camera was placed roughly 800 m from the entrance to the canal  
 245 at coordinates 43.736305°, 15.876754°. The camera was set to continuous recording at a rate of 30 fps with a resolution of  
 246 1920×1080 pixels. The camera recorded continuously, however, only recordings during daylight were useful due to the lack of  
 247 infra-red recording capability. The video files were stored locally at the camera. In total 340.5 GB were recorded over a period  
 248 of 26 days. Example image with two vessels is shown in Fig. 7. For size estimation, the length and height of two landmarks  
 were measured. These are the cretaceous limestone layer, both visible in Fig. 7.



Figure 7. Examples of an image with two vessels obtained from the video camera.

249

## 250 Vessel Detection Results by Optical Camera

### 251 Summary of Detected Vessels

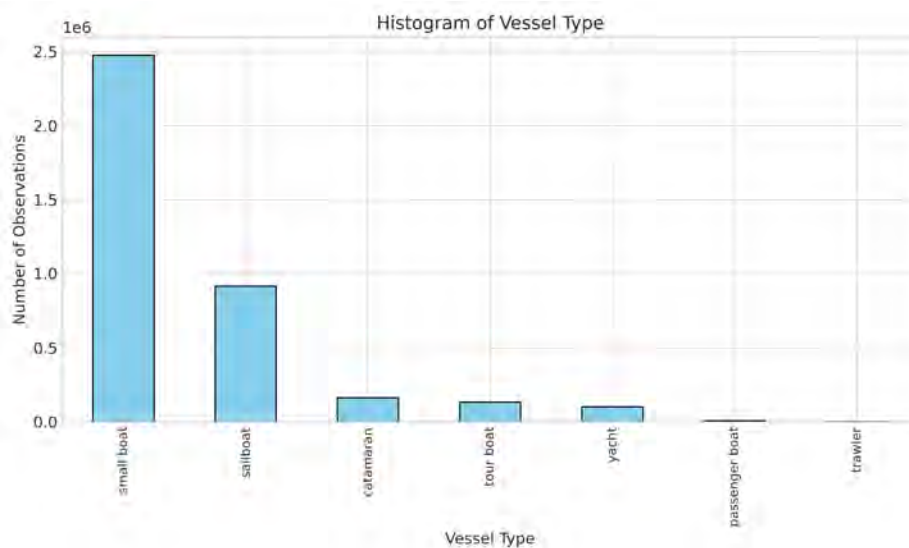
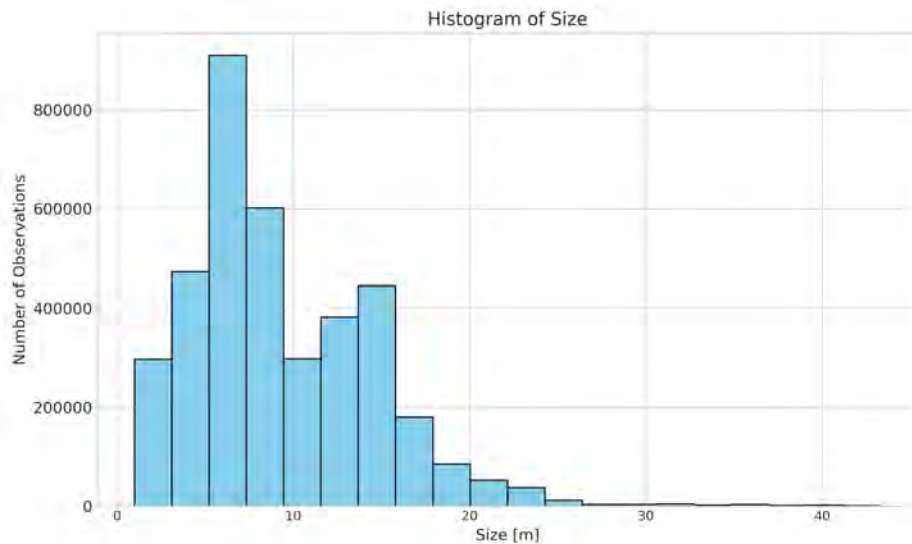


Figure 8. Histogram of vessel classes the final vessel detection result.

252 Our dataset contains 3,799,505 camera detections of various types of vessels, along with their corresponding detection  
 253 times, estimated sizes, and velocities. The histogram in Fig. 8 indicates that the "small boat" class is by far the most common

254 in this dataset, representing around 65% of all detected vessels. Additionally, sailboats are frequently observed, likely due  
255 to the presence of charter marinas in the area. A distribution of vessel sizes is presented in Fig. 9. The data reveals maxima  
256 at around 5-8 meters, which is a common size for vessels classified as small boats, and at 12-15 meters, which is typical for  
regular sailboats.



**Figure 9.** Histogram of vessels size in the final vessel detection result.

257 The histogram in Fig. 10 shows the density of vessels' velocities. We determine positive speed for vessels exiting the  
258 channel towards the port and vice versa for vessels entering the channel. Results show that vessels moving towards the port  
259 move slower compared to those heading towards open sea. Most vessels travel at an absolute speeds of  $2.5\text{--}4.0\text{ ms}^{-1}$  (4.85–7.7  
260 knots). This is expected, considering that the most frequently detected class was small boats.

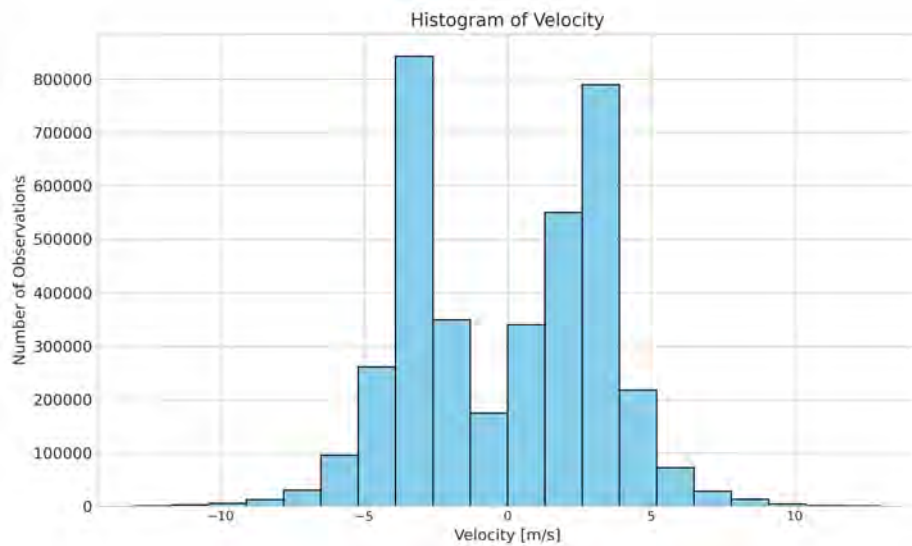


**Figure 10.** Histogram of vessels velocity in the final vessel detection result. Positive speed reflects vessels exiting the channel, and vice versa for vessels entering the channel.

261

### 262 **Results of Vessel Size and Speed Estimations**

263 To examine the algorithm's performance in estimating vessel size and velocity, a small dataset was created with the vessels of  
264 known size and speed. The picture in Fig. 11 is of a small research vessel belonging to the Institute Ruđer Bošković, with a

265 measured waterline length of 8 m and a total length of 9.3 m. To evaluate the size estimation error, the boat performed two  
 266 transactions on both the left and right sides of the channel. The images collected from 4 such passages are shown in Fig. 11.

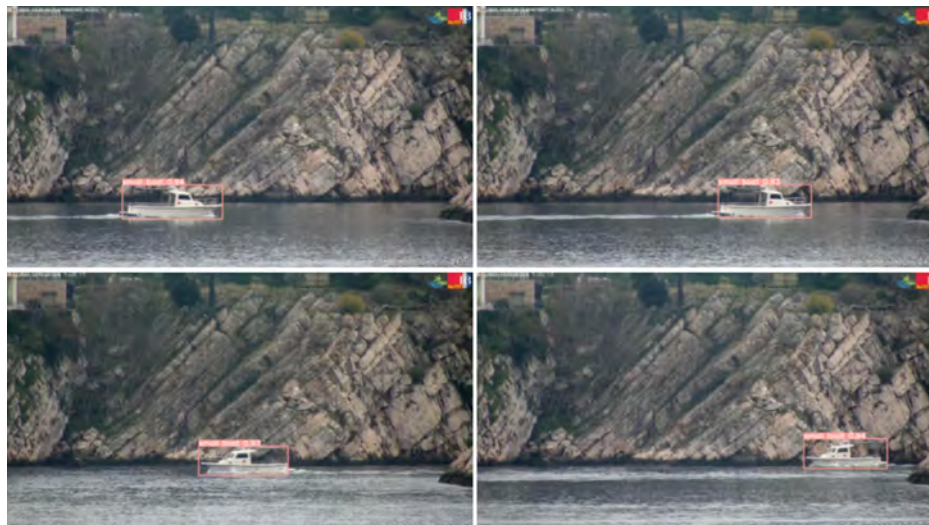


**Figure 11.** Detections on the vessel with known size for the purpose of algorithm performance evaluation.

266 Successful detection and classification occur in all frames. However, due to the angle of the vessel, the final part of the stern  
 267 is included in the bounding box of only some of the frames. Size estimation results of the test vessel for 6 corresponding frames  
 268 are given in Table 2. The average length of 8.495 m is close to the waterline length, and a standard deviation of 0.2187 m  
 269 represents roughly 3% of the average value. We deem this error acceptable considering the use of a single monocular camera.

**Table 2.** Test results for the Ruđer Bošković Research Vessel (waterline length of 8 m and total length of 9.3 m)

Video Frame	Bounding Box	Estimated Length
1	(0.357, 0.745, 0.214, 0.130)	9.15 m
2	(0.622, 0.743, 0.199, 0.126)	8.53 m
3	(0.794, 0.697, 0.178, 0.113)	7.64 m
4	(0.357, 0.745, 0.214, 0.130)	9.15 m
5	(0.611, 0.727, 0.194, 0.111)	8.33 m
6	(0.508, 0.724, 0.191, 0.111)	8.17 m
<b>Average Length</b>		8.495 m
<b>Standard Deviation</b>		0.2187 m

270

**Table 3.** Test results for length and speed estimations for 9 vessels identified by both camera and AIS

Boat Index	Length [m]	Estimated Length [m]	Velocity $\text{ms}^{-1}$	Estimated Velocity $\text{ms}^{-1}$
1	12.0	14.48696	6.1	6.99
2	12.0	12.97377	5.1	4.47
3	15.0	16.89319	6.4	6.61
4	15.0	15.37999	5.6	5.25
5	14.0	14.2389	5.0	5.25
6	14.0	14.53657	5.0	5.05
7	17.0	19.39864	6.2	5.44
8	17.0	18.65444	6.4	5.83
9	13.0	13.34587	5.2	5.05
<b>Average error</b>		7.707%		7.395%
<b>Error Std. Dev</b>		5.368%		4.855%

271 Another validation of the size and velocity measurements was performed over incidences involving vessels carrying AIS.  
 272 To this end, we filtered a large dataset of 65,000 AIS recorded at a low frame rate of 5 min within the channel. That resulted in  
 273 only 9 recordings that aligned with the camera frame allowing us to match the AIS data with the camera data accurately. This  
 274 low number of vessels emphasizes the low rate of detection available for shipping URN measurements using AIS data only.  
 275 The true and estimated size and speed of these 9 vessels are listed in Table 3. An average error of roughly 7% in both length  
 276 and speed is observed. Part of this error is due to the rounding operation of the AIS.

### 277 Results of Shipping Noise Estimation

278 Of the thousands of vessel transits recorded by the visual algorithm, 1148 passed quality control (see Section below) and  
 279 were processed to extract their acoustic characteristics, i.e., sound pressure level and 1/3 octave spectrum. Each vessel transit  
 280 was labeled according to its type, the time and date of the transit, as well as the vessel hull name and IMO number, where  
 281 applicable<sup>3</sup>. The length and speed of each transit were associated according to the calculations made by the visual algorithm.  
 282 Table 4 presents an overview of the analyzed vessels' characteristics, i.e., class, number of observations, speed, length, and  
 283 the calculated sound pressure levels at the source (SL-SPL). The largest vessel observed was a 54-meter mega-yacht named  
 284 "Premier" (IMO 9949132), while the smallest is a 3.3-meter motorboat. The fastest vessel analyzed is a motorboat sailing at  
 15.9 meters per second (m/sec), i.e., 31 knots. The slowest vessel is a sailboat sailing at 1.1 m/sec.

**Table 4.** Characteristics of the vessel dataset

Class	Number of Observations	Speed [m/sec]	Length [m]	SL-SPL [dB]
<b>Ferry</b>	50	5.66 ± 0.63	41.95 ± 6.43	178.16 ± 5.79
<b>Auxiliary Vessel</b>	1	3.5	35.77	176
<b>Cargo Vessel</b>	2	3.1 ± 0.28	44	179.45 ± 1.916
<b>Fishing Vessel</b>	2	3.60 ± 0.28	13.48 ± 6.31	167.35 ± 0.50
<b>Tour Boat</b>	63	3.44 ± 0.61	21.01 ± 2.43	167.11 ± 4.77
<b>Diving Boat</b>	1	2.80	15.33	172.22
<b>Yacht</b>	124	4.27 ± 0.96	25.65 ± 10.96	172.12 ± 5.64
<b>Sailboat</b>	192	3.22 ± 0.63	15.38 ± 4.12	162.46 ± 5.35
<b>Motor Boat</b>	713	5.15 ± 2.00	7.88 ± 2.14	170.96 ± 4.49
<b>Full Dataset</b>	<b>1148</b>	<b>4.65 ± 1.82</b>	<b>13.38 ± 9.86</b>	<b>169.79 ± 6.12</b>

285 Fig 12 presents a scatter-gram of SL-SPL for each vessel category. Among the large sample categories including "ferries",  
 286 "motorboats", "sailboats", "tour boats" and "yachts"; the "ferry" category presented the highest SL-SPL levels, followed by the  
 287 "yacht" and "motorboat" categories. The lowest mean and median SL-SPL were associated with the "sailboat" category. The  
 288 loudest vessel observed was the *Postira* ferry (IMO 6283202) sailing at 6.5 m/sec, which presented a calculated source level  
 289 of 188.26 dB; the other top 5 in terms of SL-SPL was a high-speed motorboat, other transits of *Postira* ferry and megayacht  
 290 "*Adriatica*" (IMO 9852303). The quietest vessel was a sailboat (under motor operation) sailing at 2.4 m/sec, which presented a  
 291 calculated source level of 151.91 dB; the other bottom 5 in terms of SL-SPL were also various sailboats.  
 292

293 Fig. 13 presents the one-third octave bands<sup>4</sup> for the top 5 highest-scoring SL-SPL in each major category in the dataset.  
 294 We observe that the categories "ferry", "tour boat", "motorboat", and "yacht" share a similar characteristic, with most of the  
 295 acoustic energy centering around the 80–400 Hz bands. The "motorboat" category was also characterized by sharp peaks in  
 296 specific high-frequency bands. This is likely attributed to narrow-band energy generated by the high RPM engine components  
 297 of motorboats. We also observe that the "motorboat" and "yacht" categories present significant variances between different  
 298 vessels with similar lengths and speeds within each category; the most plausible cause of this are the differences in engine  
 299 types running at different RPMs with unique transmissions. The "ferry" category<sup>5</sup> presented additional notable peaks in the 50,  
 300 630, and 1600 Hz bands. The "tour boat" category presented an additional peak in the 630 Hz band as well. The top 5 scoring  
 301 SL-SPL in the "sailboat" category also share the 80–400 Hz characteristic similar to the other categories. However, an irregular  
 302 and unique one-third octave spectrum was observed for a 15.6 m catamaran sailboat sailing at 4.1 m/sec. This specific sailboat  
 303 displays rather low one-third octave band levels overall, albeit with very high-peak narrow-band levels at the 80, 160, 1250 and  
 304 2500 Hz bands. A further audio examination by an acoustic expert attributed these high-level narrow-band noises to a possible  
 305 mechanical fault stemming from abnormal friction of the vessel's propeller shaft against the shaft bearings and sealing. This  
 306 type of noise is commonly associated with mechanical fatigue or poor maintenance and was explored in depth in the work of  
 307 Lin et al.<sup>63</sup>.

<sup>3</sup>The hull name and IMO no. were associated to a vessel transit in cases where the hull name was visible via the camera footage

<sup>4</sup>We neglected the frequency bands >31.5 Hz due to cut-off frequency effects.

<sup>5</sup>The top 5 highest SL-SPL were all associated with *Postira* ferry, hence the similarities in one-third octave graphs.

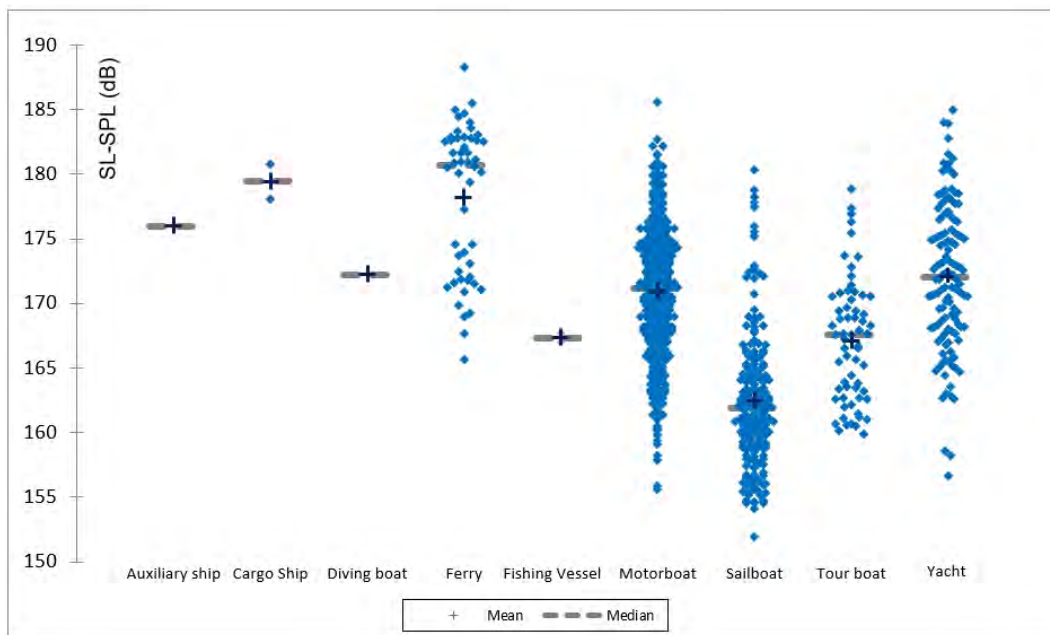


**Figure 12.** A scatter-gram of SL-SPL for all analyzed vessel categories.

308 In order to compare the one-third octave band levels in our dataset to common standards found in the shipping industry,  
 309 in Fig. 13 we compare our measured URN levels with the limit curves of Lloyd's Register "Transit" and "Silent" Notations<sup>6</sup>.  
 310 We observe that in all categories the top 5 SL-SPL scoring vessels exceed the limit curves, which were designed for much  
 311 larger vessels in most frequency bands. The following subsections delve into the statistical analysis of the impact of vessel  
 312 characteristics, such as type, length, and speed, on SL-SPL.

### 313 **Noise Estimation for Ferries**

314 A total of 50 ferry transits by 4 different ferries were evaluated: *Postira* (IMO 6283202), *Lošinjanka* (IMO 7038513), *Lara*  
 315 (IMO 8846369) and *Mali Princ* (IMO 9553189). See images in Fig. 14. A scatter plot of the relation between the calculated  
 316 SL-SPL to the speed of the vessel for each transit is given in Fig. 15a. It is apparent that for most transit speeds, the *Lošinjanka*  
 317 is the loudest ferry observed in our research; however, for transit speeds exceeding 6 m/sec, *Postira* presented the highest  
 318 SL-SPL's. *Lara* displayed the single lowest SL-SPL in the ferry category (165.63 dB); however, this measurement was also  
 319 associated with the lowest transit speed in the category (4.3 m/sec). Overall, *Mali Princ* presented the lowest SL-SPLs when  
 320 compared to the other ferries under similar transit speeds. Specifically, at around 6 m/sec, *Mali Princ* had similar SL-SPL to  
 321 that of *Lara* when operating at 5 m/sec and 5–8 dB lower than those calculated for *Lošinjanka* and *Postira*. All ferries display a  
 322 positive relation between the speed of transit and SL-SPL, albeit to a varying degree: *Lara* displays the highest regression  
 323 coefficient of speed on SL-SPL ( $\beta=8.34$ ), followed by *Postira* ( $\beta=7.14$ ) and *Mali Princ* ( $\beta=3.41$ ). *Lošinjanka* displays the  
 324 lowest regression coefficient of speed on SL-SPL ( $\beta=0.49$ ).

325 To test for statistical significance of the effect of speed on SL-SPL in the "ferry" category, in Fig. 15b we show a linear  
 326 regression model of all ferry transits<sup>7</sup>. The regression model was found to be positive and statistically significant ( $R^2 = 0.393$ ),  
 327  $F(1,48) = 31.478$ ,  $p < 0.0001$ .

### 328 **Noise Estimation for Tour Boats**

329 Some of the medium-sized vessels observed in the testbed conducted regular transits at similar hours on a nearly daily basis.  
 330 These vessels were observed carrying a large number of people on the deck, see example in Fig. 16. We, therefore, classified  
 331 these vessels as "Tour Boats". Our dataset includes a total of 64 transits by 9 distinct tour boats<sup>8</sup>. Fig. 17a provides a scatter  
 332 plot of speed to SL-SPL for the various tour boats, and Fig. 17b shows a linear regression model for all tour boats observed.  
 333 The regression model was found to be positive and statistically significant ( $R^2 = 0.55$ ),  $F(1,61) = 75.902$ ,  $p < 0.0001$ . Most

<sup>6</sup>Lloyd's Register is one of the largest shipping classification societies in the world. In 2018, Lloyd's introduced two URN mitigation notations that can be applied to vessels that comply with specific URN requirements, i.e., a one-third octave noise spectrum not exceeding specified limit curves<sup>18</sup>.

<sup>7</sup>Speed of transit was the only independent variable chosen in the "ferry" category due to the repetitive nature of the length variable.

<sup>8</sup>By reviewing the camera footage, it is possible to differentiate between the different types of tour boats; however, as there are no visible hull names, we chose to name them in a random order from A to J

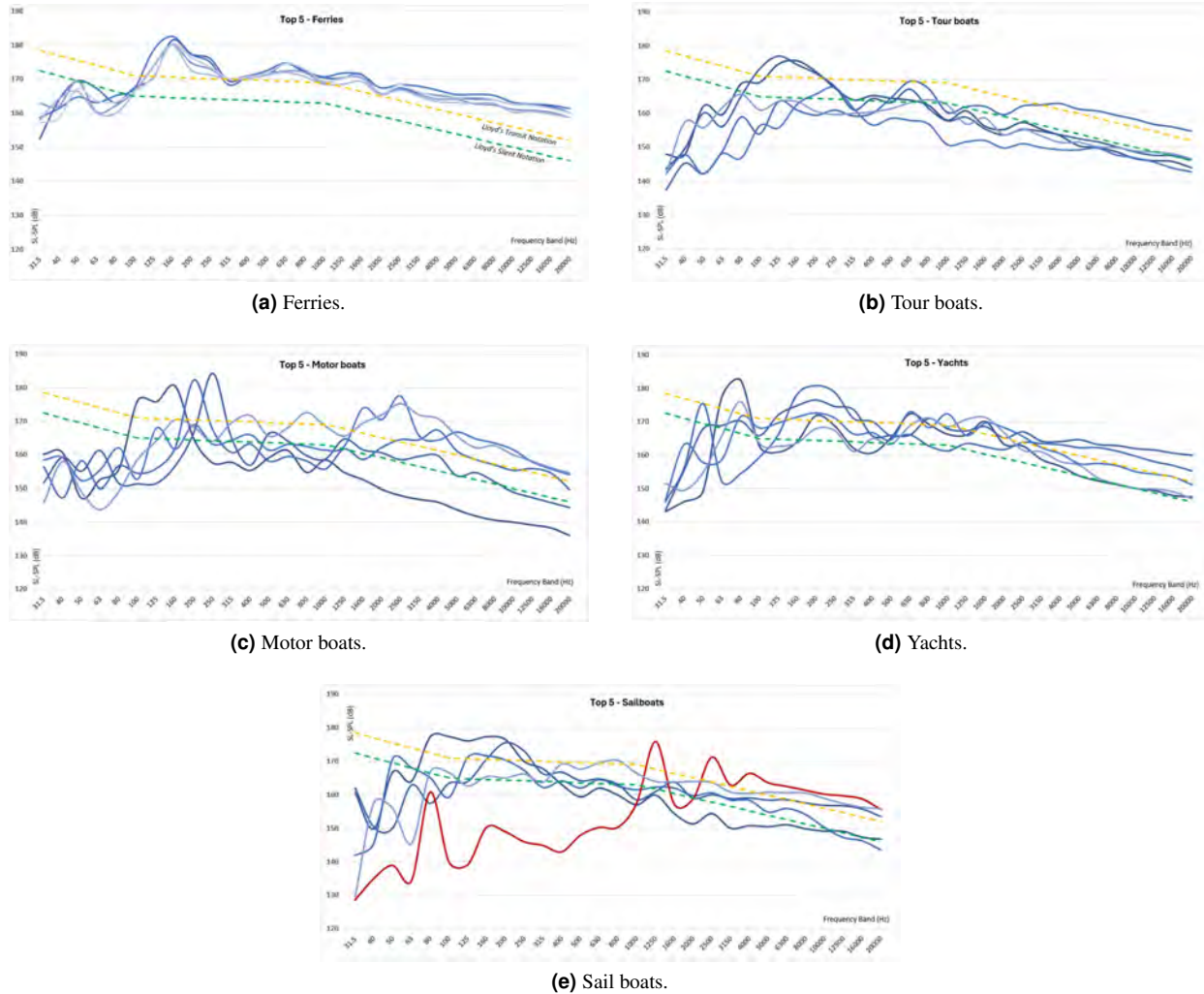


**Figure 13.** One-third octave bands compared to Lloyd's Register URN limit curves for "Transit" and "Silent" Notations.

334 tour boats share similar regression coefficients for speed on SL-SPL ( $\beta \approx 4.5$ ). A visual comparison of tour boats reveals that  
 335 most of them share many similarities in hull design and length, which may also indicate a similarity in their propulsion systems;  
 336 this offers a plausible explanation for the similarities in their speed regression coefficients. A prominent exception can be seen  
 337 for Tour boat A, which has a unique hull design (and the highest number of observations); its regression coefficient was found  
 338 to be higher ( $\beta = 12.17$ ).

339 **Noise Estimation for Yachts**

340 A total of 124 yacht transits were evaluated as part of the research. As there is no clear and acceptable standard for classifying a  
 341 recreational vessel as a "Yacht," we chose to classify any recreational motor vessel longer than 15 m as a "Yacht"<sup>9</sup>. See example  
 342 in Fig. 18.

343 To assess the effect of yacht speed and size on SL-SPL, a multivariate linear regression model is given in Fig. 19. The  
 344 regression was found to be positive and statistically significant ( $R^2 = 0.29$ ),  $F(2, 121) = 25.25$ ,  $p < 0.0001$ . Additionally, it  
 345 was found that speed has a more prominent effect on SL-SPL ( $\beta = 2.33$ ) than the length of the vessel ( $\beta = 0.23$ ).

346 **Noise Estimation for Sailboats**

347 A total of 192 sailboats that were observed under motor operation were assessed. Most of the analyzed sailboats (n=180) can be  
 348 categorized as modern mono-hull and catamaran sloops ranging from 7–20 m in length, which are regularly found near coastal  
 349 marinas, the other type of sailboats were larger (>30 m) with multiple masts and more elaborate rigging, e.g., Schooners and

<sup>9</sup>The 15 m consideration was taken from online sources engaged in the recreational vessel business<sup>64</sup>.



**Figure 14.** The different ferries encountered in the testbed - from upper-left clockwise - "*Mali Princ*", "*Lošinjanka*", "*Lara*" and "*Postira*"

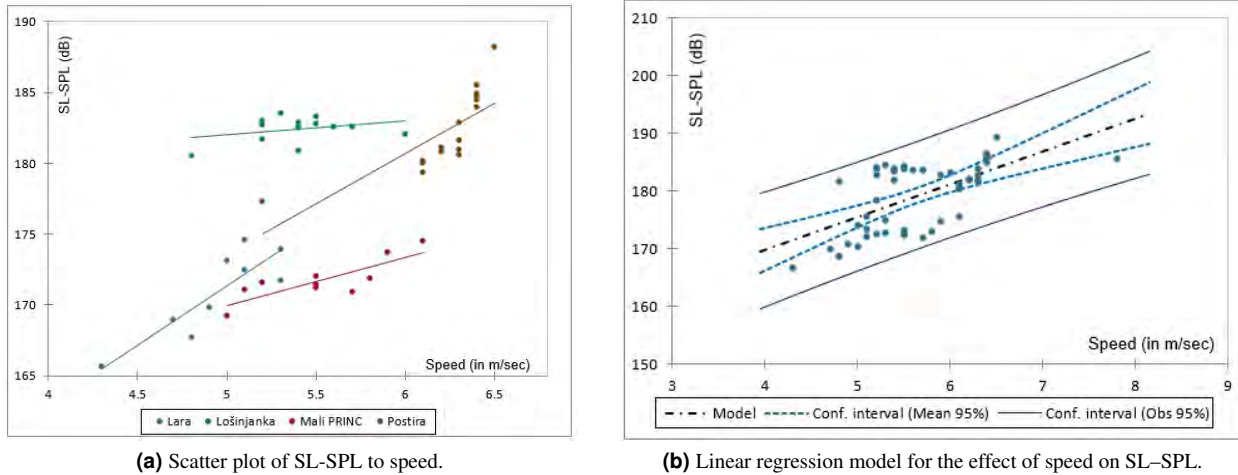


**Figure 15.** Scatter plot and Linear regression model of the ferry category.

350 Cutters. See examples in Fig. 20.

351 A multivariate linear regression model for the relation between the sailboats' SL-SPL and their speed and length is given  
 352 in Fig. 21. The regression was found to be positive and statistically significant ( $R^2 = 0.40$ ),  $F(2, 189) = 63.45$ ,  $p < 0.0001$ .  
 353 Additionally, it was found that speed has a more larger regression coefficient (i.e., a more prominent effect on SL-SPL)  
 354 ( $\beta = 4.86$ ) than the length of the vessel ( $\beta = 0.58$ ).

355 The "Sailboat" category scored the lowest SL-SPL mean among all vessel categories. This coincides with the fact that the  
 356 engine system on sailboats are usually not the main source of propulsion but rather acts primarily as a support propulsion for  
 357 entering and exiting the harbor or in cases where wind conditions are unfavorable. Regarding the differences between hull  
 358 designs (mono hull vs. catamaran), a meta-analysis conducted by Parson et al.<sup>65</sup> showed that catamaran hulls tended to display





**Figure 16.** An example of tour boats observed in the testbed: Tour boat A (left) and Tour boat E (right)

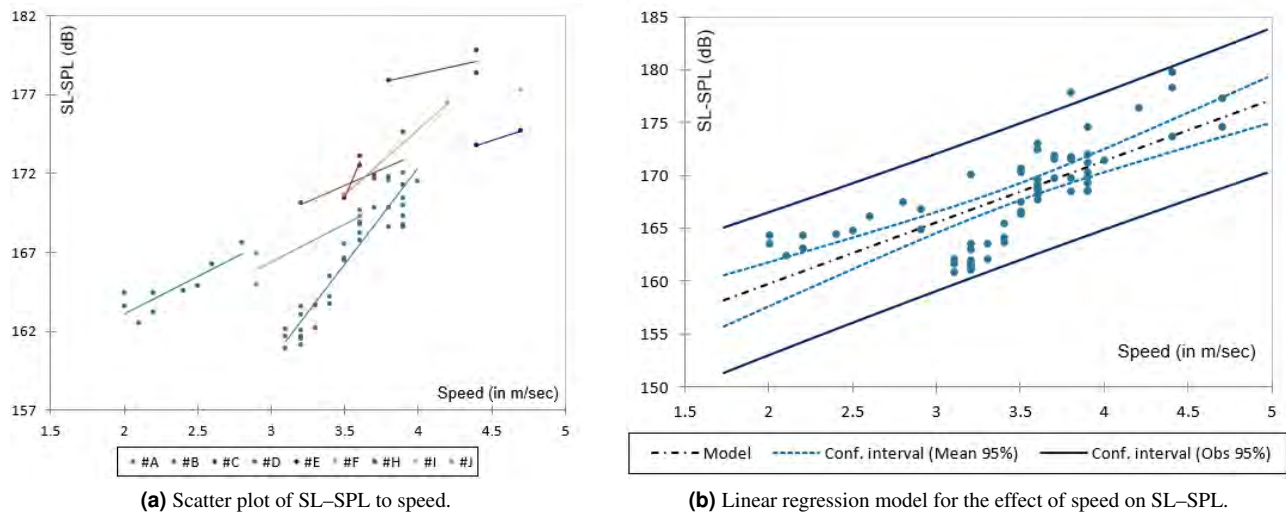


**Figure 17.** The "Tour boat" category.



**Figure 18.** An example of yachts observed in the testbed: From left to right, a 15 m mono hull cruiser and the *Zeus* megayacht (IMO 9878187).

359 higher SL-SPL than mono hulls. In order to statistically test the mean differences of mono hull vs. catamaran SL-SPL's while  
 360 controlling for length and speed, we performed an analysis of covariance (ANCOVA) test between mono hull and catamaran  
 361 sailboats. The results indicate that the speed has a statistically significant effect on SL-SPL,  $F(3, 176) = 62.38, p < 0.0001$ ,

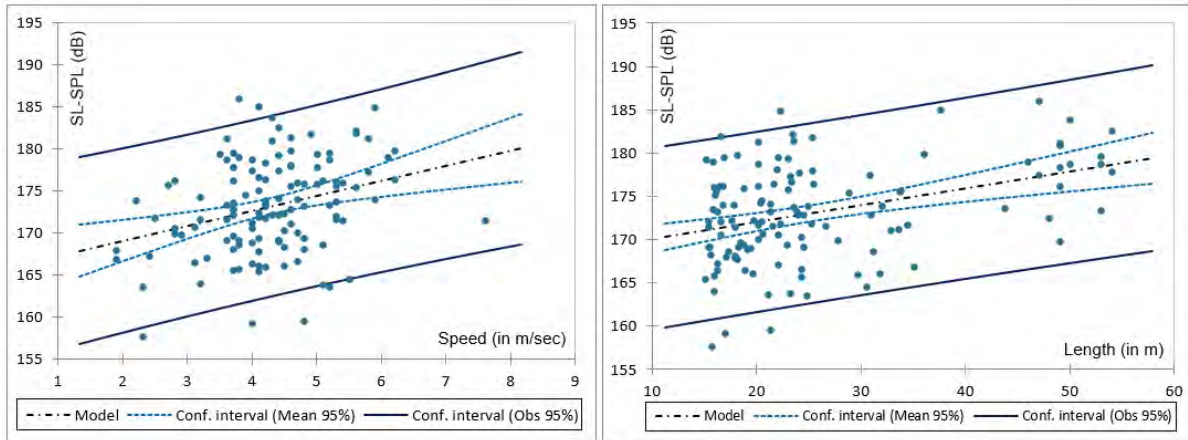


**Figure 19.** Multivariate linear regression model for the effect of speed (left) and length (right) on SL-SPL in the "Yacht" category.



**Figure 20.** An example of sailboats observed in the test bed - a 33m Schooner (left) and a 15m monohull modern sloop (right)

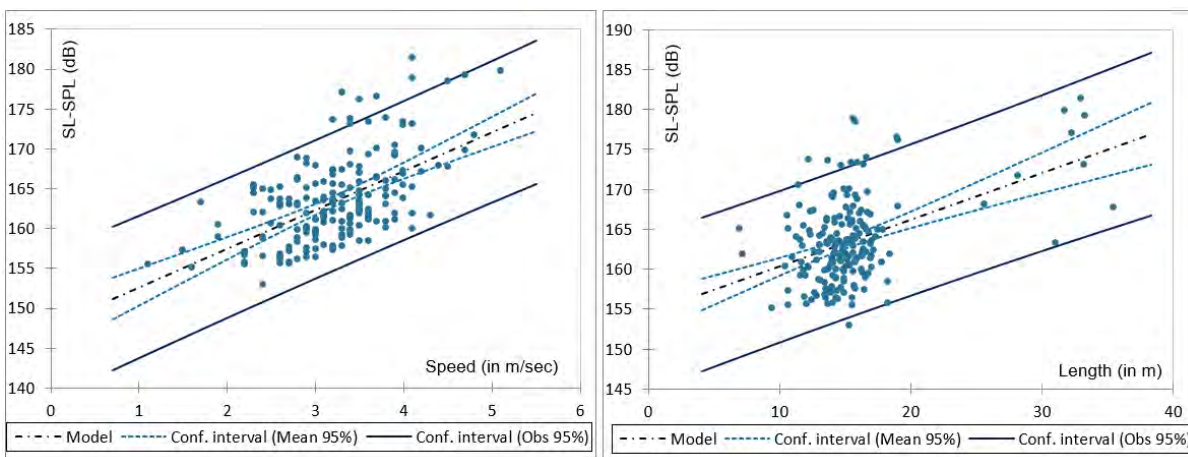


**Figure 21.** Multivariate linear regression model for the effect of speed (left) and length (right) on SL-SPL in the "Sailboat" category

362 which coincides with the above linear regression model. As expected, due to the minute differences between the mean length of

363 catamaran and mono hull sailboats, the length had no significant effect on SL-SPL,  $F(1, 176) = 0.068, p < 0.795$ . Regarding  
 364 the hull design, the ANCOVA test has shown that it does not have any significant effect on SL-SPL when controlling for speed  
 365 and length,  $F(1, 176) = 0.018, p < 0.895$ .

366 **Noise Estimation for Motorboats**

367 The "Motorboat" category is the largest in our dataset, with 713 transits. We classified motorboats as all types of engine-propelled  
 vessels under 15 m with no alternative propulsion methods (e.g., sails). See examples in Fig. 22.

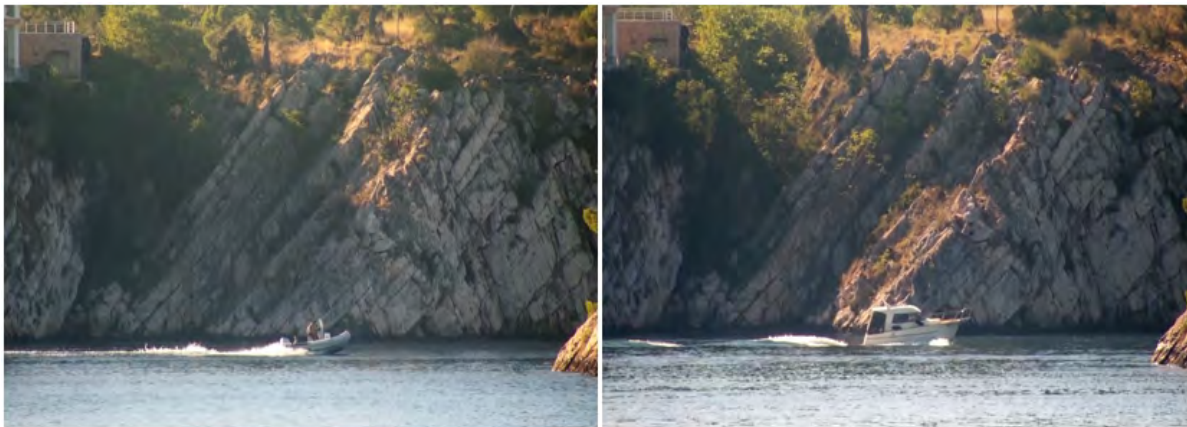


**Figure 22.** An example of motorboats observed in the testbed: a 5.4 m outboard engine motorboat at 9.8 m/sec (left) and an 8.9 m inboard engine motorboat at 4.7 m/sec (right)

368 It is important to note that the second highest SL-SPL calculated in the entire dataset was an outboard engine motorboat  
 369 cruising at 11.5 m/sec (22.35 knots) with an SL-SPL of 185.55 dB. This infers that motorboats cruising at high speeds may  
 370 display SL-SPL's comparable or even higher than those of much larger vessels at their nominal transit speeds.  
 371

372 A multivariate linear regression for the effect of speed and length on SL-SPL in the "Motorboat" category is given in  
 373 Fig. 23. The model was found to be positive and statistically significant ( $R^2 = 0.18$ ),  $F(2, 710) = 76.881, p < 0.0001$ . To  
 374 further explore any other variables that may affect SL-SPL, we performed another sub-categorization of the motorboat dataset  
 375 into two sub-groups: outboard engine-powered and inboard engine-powered. An ANCOVA test for the effect of the engine type  
 376 on SL-SPL's while controlling for length and speed showed that there is no statistically significant effect of the type of engine  
 (inboard/outboard) on SL-SPL,  $F(3, 709) = 1.562, p < 0.212$ .

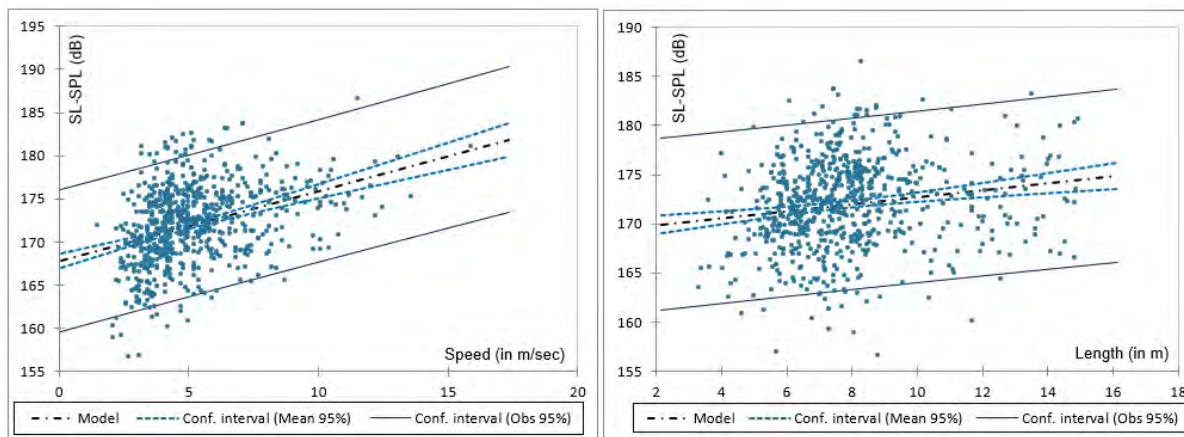


**Figure 23.** Multivariate linear regression for Motorboats

377

378 **Usage Notes**

379 Overall, 1148 vessel transits were evaluated. As mentioned in Sec., URN calculations for small vessels in the coastal area  
 380 have been mostly absent from the current research agenda, primarily due to the lack of any open-source information systems

381 that broadcast vessel data (e.g., AIS found on larger commercial vessels). This, in turn, creates inherent difficulties in  
382 collecting vessel parameters, e.g., length and speed, which are crucial parameters for URN calculations. In this sense, the novel  
383 methodology implemented in this research framework enabled the formation of what can be considered the most comprehensive  
384 dataset to date, specifically focused on small to medium vessels.

385 The dataset leads to several significant insights. Firstly, SL-SPLs are highly dependent on the vessel characteristics. As  
386 expected, speed was found to have a statistically significant and strong effect on SL-SPL for all vessel types. The vessel's  
387 length was also shown to have a statistically significant effect on SL-SPL, albeit to a lesser degree. This can be explained by  
388 the larger propellers required for these vessels and to the the greater displacement of water by large vessels. However, the  
389 relatively moderate  $R^2$  values, especially in the "Motorboat" category ( $R^2 = 0.18$ ), may reflect a dependency on other unknown  
390 independent variables such as variations in the engine design and output power rating. Secondly, comparing the SL-SPLs of  
391 different types of vessels has shown that small recreational boats may emit SL-SPLs as high as much larger ships. For instance,  
392 we observed a 8.3 m motorboat sailing at 11.5 m/s with SL-SPL comparable to that of a 45 m ferry sailing at 6.4 m/s. These  
393 findings coincide with previous findings<sup>26,32,50</sup>. However, the result of the ANCOVA test for subgroups of vessels of the same  
394 type revealed no statistical significance on SL-SPL. Thirdly, observing one-third octave spectrum levels, most of the URN  
395 energy were primarily centered around the 80–400 Hz band. Still, unique characteristics were found for some categories, e.g.  
396 motorboats that presented high-frequency narrow-band peaks. A specifically intriguing spectrum was found in the "Sailboat"  
397 category, with a catamaran sailboat with a possible mechanical fault (i.e., abnormal friction in propeller shaft) that caused it  
398 to generate higher SL-SPL compared to other sailboats with a similar design (catamaran) with similar lengths and speeds.  
399 Comparing our finding against the Lloyd's "Transit" and "Silent" notations, we found that the small vessels in our dataset  
400 display levels exceeding the standards designed for much larger vessels. These conclusions point on the critical need to expand  
401 the URN research agenda to include small vessels. This is not only because such vessels are increasingly prevalent in coastal  
402 waters, but also because they may contribute more noise pollution to the water than the large cargo vessels that have been the  
403 primary focus of the current URN research agenda.

404 In making our database of URN of VOO, our biggest concern was the averaging window around the CPA for URN  
405 estimation. The size of this window should be long enough to suppress noise but also short enough to avoid differences in the  
406 received power due to the changing distances between the receiver and the moving vessel. In our database, we have followed the  
407 method recommended in ISO 17208<sup>48</sup> that manages this trade-off by setting the observation window as the time-frame in which  
408 the vessel passes the  $\pm 30^\circ$  aspect tangent to the hydrophone. However, for some of the fast motorboats sailing at  $>10$  m/sec,  
409 this resulted in relatively short time-window lengths ( $\sim 4$  s). A possible way to address this challenge is a statistical measure to  
410 test the stability of the acoustic intensity around the CPA and to determine the size of the observation time accordingly.

411 Another challenge encountered is the extensive traffic of vessels within the channel where the recordings took place. To  
412 avoid any mutual interference caused by vessels transiting the channel in close proximity, we placed a strict quality control  
413 process (see Section below) and dismissed cases identified by the video footage or acoustics of vessels transiting the channel in  
414 close proximity. As a result, roughly 90% of the vessel transits did not pass quality control. The case of too close vessels also  
415 poses a challenge for monitoring the URN of VOO in realistic conditions of near port measurements. Future work will address  
416 this challenge by incorporating noise cancellation techniques such as the method in<sup>66</sup>.

## 417 Code availability

418 Processing code can be available upon request.

## 419 References

- 420 1. Wenz, G. M. Acoustic ambient noise in the ocean: Spectra and sources. *The journal acoustical society Am.* **34**, 1936–1956  
421 (1962).
- 422 2. Hildebrand, J. A. Anthropogenic and natural sources of ambient noise in the ocean. *Mar. Ecol. Prog. Ser.* **395**, 5–20  
423 (2009).
- 424 3. Southall, B. L. *et al.* Underwater noise from large commercial ships—international collaboration for noise reduction.  
425 *Encycl. Marit. Offshore Eng.* 1–9 (2017).
- 426 4. Erbe, C. *et al.* The effects of ship noise on marine mammals—a review. *Front. Mar. Sci.* **6**, 476898 (2019).
- 427 5. Gordon, J. *et al.* A review of the effects of seismic surveys on marine mammals. *Mar. Technol. Soc. J.* **37**, 16–34 (2003).
- 428 6. Nelms, S. E., Piniak, W. E., Weir, C. R. & Godley, B. J. Seismic surveys and marine turtles: An underestimated global  
429 threat? *Biol. conservation* **193**, 49–65 (2016).
- 430 7. Blom, E.-L. *et al.* Continuous but not intermittent noise has a negative impact on mating success in a marine fish with  
431 paternal care. *Sci. reports* **9**, 5494 (2019).

- 432 **8.** Buscaino, G. *et al.* Impact of an acoustic stimulus on the motility and blood parameters of european sea bass (*dicentrarchus*  
433 *labrax* l.) and gilthead sea bream (*sparus aurata* l.). *Mar. environmental research* **69**, 136–142 (2010).
- 434 **9.** Carter, E. E., Tregenza, T. & Stevens, M. Ship noise inhibits colour change, camouflage, and anti-predator behaviour in  
435 shore crabs. *Curr. Biol.* **30**, R211–R212 (2020).
- 436 **10.** Diamant, R., Testolin, A., Shachar, I., Galili, O. & Scheinin, A. Observational study on the non-linear response of dolphins  
437 to the presence of vessels. *Sci. Reports* **14**, 6062 (2024).
- 438 **11.** Erbe, C., MacGillivray, A. & Williams, R. Mapping cumulative noise from shipping to inform marine spatial planning.  
439 *The J. Acoust. Soc. Am.* **132**, EL423–EL428 (2012).
- 440 **12.** Casale, P. *et al.* Mediterranean sea turtles: current knowledge and priorities for conservation and research. *Endangered*  
441 *species research* **36**, 229–267 (2018).
- 442 **13.** Sèbe, M., Christos, A. K. & Pendleton, L. A decision-making framework to reduce the risk of collisions between ships and  
443 whales. *Mar. Policy* **109**, 103697 (2019).
- 444 **14.** Jensen, F. H. *et al.* Vessel noise effects on delphinid communication. *Mar. Ecol. Prog. Ser.* **395**, 161–175 (2009).
- 445 **15.** Arveson, P. T. & Vendittis, D. J. Radiated noise characteristics of a modern cargo ship. *The J. Acoust. Soc. Am.* **107**,  
446 118–129 (2000).
- 447 **16.** Audoly, C. & Meyer, V. Measurement of radiated noise from surface ships-influence of the sea surface reflection coefficient  
448 on the lloyd’s mirror effect. In *ACOUSTICS 2017* (2017).
- 449 **17.** CMRE. Sonar acoustics handbook by center for maritime research & experimentation (CMRE). In *Animal communication*  
450 *and noise*, 20–23 (UComms 18 special edition, 2018).
- 451 **18.** Lloyd’s, R. LR announces new underwater noise notation. [https://www.lr.org/en/knowledge/press-room/press-listing/  
452 press-release/lr-announces-new-underwater-noise-notation/](https://www.lr.org/en/knowledge/press-room/press-listing/press-release/lr-announces-new-underwater-noise-notation/) (2018). [Accessed 01-07-2024].
- 453 **19.** Gassmann, M., Wiggins, S. M. & Hildebrand, J. A. Deep-water measurements of container ship radiated noise signatures  
454 and directionality. *The journal acoustical society Am.* **142**, 1563–1574 (2017).
- 455 **20.** Zhu, C., Gaggero, T., Makris, N. C. & Ratilal, P. Underwater sound characteristics of a ship with controllable pitch  
456 propeller. *J. Mar. Sci. Eng.* **10**, 328 (2022).
- 457 **21.** Salio, M. P. Numerical assessment of underwater noise radiated by a cruise ship. *Ships Offshore Struct.* **10**, 308–327  
458 (2015).
- 459 **22.** Grelowska, G., Kozaczka, E., Kozaczka, S. & Szymczak, W. Underwater noise generated by a small ship in the shallow  
460 sea. *Arch. Acoust.* **38**, 351–356 (2013).
- 461 **23.** McKenna, M. F., Ross, D., Wiggins, S. M. & Hildebrand, J. A. Underwater radiated noise from modern commercial ships.  
462 *The J. Acoust. Soc. Am.* **131**, 92–103 (2012).
- 463 **24.** Allen, J. K., Peterson, M. L., Sharrard, G. V., Wright, D. L. & Todd, S. K. Radiated noise from commercial ships in the  
464 gulf of maine: Implications for whale/vessel collisions. *The J. Acoust. Soc. Am.* **132**, EL229–EL235 (2012).
- 465 **25.** Merchant, N. D., Blondel, P., Dakin, D. T. & Dorocicz, J. Averaging underwater noise levels for environmental assessment  
466 of shipping. *The J. Acoust. Soc. Am.* **132**, EL343–EL349 (2012).
- 467 **26.** Veirs, S., Veirs, V. & Wood, J. D. Ship noise extends to frequencies used for echolocation by endangered killer whales.  
468 *PeerJ* **4**, e1657 (2016).
- 469 **27.** Zhang, G., Forland, T. N., Johnsen, E., Pedersen, G. & Dong, H. Measurements of underwater noise radiated by commercial  
470 ships at a cabled ocean observatory. *Mar. Pollut. Bull.* **153**, 110948 (2020).
- 471 **28.** ZoBell, V. M. *et al.* Underwater noise mitigation in the santa barbara channel through incentive-based vessel speed  
472 reduction. *Sci. reports* **11**, 18391 (2021).
- 473 **29.** USCG. Solas chapter v, regulation 19. <https://www.navcen.uscg.gov/sites/default/files/pdf/AIS/SOLAS.V.19.2.1-5.pdf>  
474 (2023). (Accessed on 07/02/2024).
- 475 **30.** UNCTADstat Data Centre — unctadstat.unctad.org. <https://unctadstat.unctad.org/datacentre/dataviewer/US.MerchantFleet>.  
476 [Accessed 10-06-2024].
- 477 **31.** USCG. 2022 recreational boating statistics (2023). Accessed on 01-07-2024.
- 478 **32.** Cope, S. *et al.* Multi-sensor integration for an assessment of underwater radiated noise from common vessels in san  
479 francisco bay. *The J. Acoust. Soc. Am.* **149**, 2451–2464 (2021).

- 480 **33.** Picciulin, M. *et al.* Characterization of the underwater noise produced by recreational and small fishing boats (< 14 m) in  
481 the shallow water of the cres-lošinj natura 2000 sci. *Mar. pollution bulletin* **183**, 114050 (2022).
- 482 **34.** Tran, T.-H. & Le, T.-L. Vision based boat detection for maritime surveillance. In *2016 International Conference on*  
483 *Electronics, Information, and Communications (ICEIC)*, 1–4 (IEEE, 2016).
- 484 **35.** Bao, X., Zinger, S., Wijnhoven, R. *et al.* Ship detection in port surveillance based on context and motion saliency analysis.  
485 In *Video Surveillance and Transportation Imaging Applications*, vol. 8663, 87–94 (SPIE, 2013).
- 486 **36.** Dong, C., Liu, J.-H., Xu, F., Wang, R.-H. *et al.* Fast ship detection in optical remote sensing images. *J. Jilin Univ.*  
487 *(Engineering Technol. Ed.)* (2019).
- 488 **37.** Li, H. & Man, Y. Moving ship detection based on visual saliency for video satellite. In *2016 IEEE International Geoscience*  
489 *and Remote Sensing Symposium (IGARSS)*, 1248–1250, DOI: [10.1109/IGARSS.2016.7729316](https://doi.org/10.1109/IGARSS.2016.7729316) (2016).
- 490 **38.** Spagnolo, P., Filieri, F., Distanto, C., Mazzeo, P. L. & D’Ambrosio, P. A new annotated dataset for boat detection and  
491 re-identification. In *2019 16th IEEE International Conference on Advanced Video and Signal Based Surveillance (AVSS)*,  
492 1–7, DOI: [10.1109/AVSS.2019.8909831](https://doi.org/10.1109/AVSS.2019.8909831) (2019).
- 493 **39.** Zwemer, M. H., Wijnhoven, R. G. & de With, P. H. Ship detection in harbour surveillance based on large-scale data and  
494 cnns. In *VISIGRAPP (5: VISAPP)*, 153–160 (2018).
- 495 **40.** Li, H., Deng, L., Yang, C., Liu, J. & Gu, Z. Enhanced yolo v3 tiny network for real-time ship detection from visual image.  
496 *IEEE Access* **9**, 16692–16706, DOI: [10.1109/ACCESS.2021.3053956](https://doi.org/10.1109/ACCESS.2021.3053956) (2021).
- 497 **41.** Lu, Y. *et al.* Fusion of camera-based vessel detection and AIS for maritime surveillance. In *2021 26th International*  
498 *Conference on Automation and Computing (ICAC)*, 1–6 (IEEE, 2021).
- 499 **42.** Gülsoylu, E., Koch, P., Yildiz, M., Constapel, M. & Kelm, A. P. Image and AIS data fusion technique for maritime  
500 computer vision applications. In *Proceedings of the IEEE/CVF Winter Conference on Applications of Computer Vision*,  
501 859–868 (2024).
- 502 **43.** Correia, A., Ferreira, F. & Mišković, N. Comparing different yolo versions for boat detection and classification in real  
503 datasets. In *OCEANS 2024 Singapore* (IEEE, 2024). Accepted for publication.
- 504 **44.** Jocher, G. Ultralytics yolov5. <https://github.com/ultralytics/yolov5>, DOI: [10.5281/zenodo.3908559](https://doi.org/10.5281/zenodo.3908559) (2020). Version = 7.0.
- 505 **45.** Wang, C.-Y. *et al.* Cspnet: A new backbone that can enhance learning capability of cnn. In *2020 IEEE/CVF Conference on*  
506 *Computer Vision and Pattern Recognition Workshops (CVPRW)*, 1571–1580, DOI: [10.1109/CVPRW50498.2020.00203](https://doi.org/10.1109/CVPRW50498.2020.00203)  
507 (2020).
- 508 **46.** He, K., Zhang, X., Ren, S. & Sun, J. Spatial pyramid pooling in deep convolutional networks for visual recognition. *IEEE*  
509 *Transactions on Pattern Analysis Mach. Intell.* **37**, 1904–1916, DOI: [10.1109/TPAMI.2015.2389824](https://doi.org/10.1109/TPAMI.2015.2389824) (2015).
- 510 **47.** Bewley, A., Ge, Z., Ott, L., Ramos, F. & Upcroft, B. Simple online and realtime tracking. In *2016 IEEE international*  
511 *conference on image processing (ICIP)*, 3464–3468 (IEEE, 2016).
- 512 **48.** for Standardization, I. O. Iso/dis 17208-3(en) underwater acoustics — quantities and procedures for description and  
513 measurement of underwater sound from ships — part 3: Requirements for measurements in shallow water. <https://www.iso.org/obp/ui/en/#iso:std:iso:17208:-3:dis:ed-1:v1:en> (2019). [Accessed 10-06-2024].
- 515 **49.** Jensen, F. B., Kuperman, W. A., Porter, M. B., Schmidt, H. & Tolstoy, A. *Computational ocean acoustics*, vol. 2011  
516 (Springer, 2011).
- 517 **50.** Pine, M. K., Jeffs, A. G., Wang, D. & Radford, C. A. The potential for vessel noise to mask biologically important sounds  
518 within ecologically significant embayments. *Ocean. & Coast. Manag.* **127**, 63–73 (2016).
- 519 **51.** Bahtiarian, M. A. Asa standard goes underwater. *Acoust. Today* **5**, 26–29 (2009).
- 520 **52.** Mahanty, M. M., Latha, G., Raguraman, G., Venkatesan, R. *et al.* Passive acoustic detection of distant ship crossing signal  
521 in deep waters using wavelet denoising technique. In *OCEANS 2022-Chennai*, 1–5 (IEEE, 2022).
- 522 **53.** Song, G. *et al.* Underwater noise classification based on support vector machine. In *2021 OES China Ocean Acoustics*  
523 *(COA)*, 410–414 (IEEE, 2021).
- 524 **54.** ANSI. ANSI/ASA S1.11-2014/Part 1 / IEC 61260:1-2014 - Electroacoustics - Octave-band and Fractional-octave-band  
525 Filters - Part 1: Specifications (a nationally adopted international standard — webstore.ansi.org. <https://webstore.ansi.org/standards/asa/ansiasas1112014partiec61260> (2014). [Accessed 10-06-2024].
- 526 **55.** Marsh, H. & Schulkin, M. *Underwater sound transmission* (Avco Corporation, Marine Electronics Office, 1962).
- 527

- 528 **56.** Jankowski, D., Lamm, A. & Hahn, A. Determination of ais position accuracy and evaluation of reconstruction methods for  
529 maritime observation data. *IFAC-PapersOnLine* **54**, 97–104 (2021).
- 530 **57.** Ainslie, M. A. & McColm, J. G. A simplified formula for viscous and chemical absorption in sea water. *The J. Acoust. Soc.*  
531 *Am.* **103**, 1671–1672 (1998).
- 532 **58.** Hermannsen, L., Beedholm, K., Tougaard, J. & Madsen, P. T. High frequency components of ship noise in shallow water  
533 with a discussion of implications for harbor porpoises (*phocoena phocoena*). *The J. Acoust. Soc. Am.* **136**, 1640–1653  
534 (2014).
- 535 **59.** Huljek, L., Strmić Palinkaš, S., Fiket, Ž. & Fajković, H. Environmental aspects of historical ferromanganese tailings in the  
536 šibenik bay, croatia. *Water* **13**, 3123 (2021).
- 537 **60.** Erbe, C. Underwater acoustics: noise and the effects on marine mammals. *A Pocket Handb.* **164**, 10–35 (2011).
- 538 **61.** Sipilä, T., Viitanen, V., Uosukainen, S. & Klose, R. Shallow water effects on ship underwater noise measurements. In  
539 *48th International Congress and Exhibition on Noise Control Engineering, INTER-NOISE 2019*, 1707 (Institute of Noise  
540 Control Engineering, 2019).
- 541 **62.** Shipton, M. *et al.* Hear my ship: database for vessel underwater radiated noise. <https://hearmyship.fer.hr> (2024). [Accessed  
542 21-08-2024].
- 543 **63.** Lin, C.-G., Zou, M.-S., Sima, C., Liu, S.-X. & Jiang, L.-W. Friction-induced vibration and noise of marine stern tube  
544 bearings considering perturbations of the stochastic rough surface. *Tribol. Int.* **131**, 661–671 (2019).
- 545 **64.** Islands, W. Boat vs Yacht: What are the Differences? | WI Yachts — windward-islands.net. <https://www.windward-islands.net/blog/yacht-vs-boat-differences/> (2023). [Accessed 15-06-2024].
- 547 **65.** Parsons, M. J., Erbe, C., Meekan, M. G. & Parsons, S. K. A review and meta-analysis of underwater noise radiated by  
548 small (< 25 m length) vessels. *J. Mar. Sci. Eng.* **9**, 827 (2021).
- 549 **66.** Diamant, R. Robust interference cancellation of chirp and cw signals for underwater acoustics applications. *IEEE Access*  
550 **6**, 4405–4415 (2018).

## 551 **Acknowledgements**

552 The authors would like to thank Shlomi Dahan and Mak Gračić for their help in acquiring the acoustic data, and to Matej  
553 Radović and Đula Nađ for their help in setting up the web front.

554 This research was supported by a scholarship sponsored by the Israeli Science Foundation (grant #973/23), by the University  
555 of Haifa's Innovation & Sustainability Division, and by the Horizon Europe program of the European Union under the  
556 UWIN-LABUST project (project #101086340).

## 557 **Author contributions statement**

558 MS analyzed the acoustic data, created the database and wrote the manuscript; JO and FF analyzed the visual data and wrote the  
559 manuscript; NM assisted with administration, provided funding and edited the manuscript; TB and NB acquired the acoustic  
560 and visual data; RD supervised the project, acquired the acoustic dataset, provided funding and wrote the manuscript.

## 561 **Competing interests**

562 The author(s) declare no competing interests.